Industrial Engineering & Management

Citarella et al., Ind Eng Manage 2015, 4:2
DOI: 10.4172/2169-0316.1000160

Research Article Open Access

# Fatigue Crack Growth by FEM-DBEM Approach in a Steam Turbine Blade

**Citarella R[1]*, Lepore M[2], Shlyannikov M[2] and Yarullin R[2]**

[1]Department of Industrial Engineering, University of Salerno, via Giovanni Paolo II, 132, Fisciano (SA), Italy
[2]Kazan Scientific Centre of Russian Academy of Sciences, Lobachevsky Street, 2/31, 420111, Kazan, Russia

## Abstract

This study is concerned with the integrity assessment of cracked steam turbine rotor components, made of steel X20Cr13, that operate under cyclic loading. Damage accumulation and growth occurred on the leading edge of turbine blade starting from part-through surface flaws. Tensile tests are performed for assessment of the main mechanical and fracture steel properties: specimens are cut out from critical zones of turbine blade body after a given operating time. The subject for experimental studies is a steel bar of circular cross-section with straight-fronted edge crack. The optical microscope measurement and the COD method are used to monitor crack growth during the tests. An automatic crack propagation simulation on the blade is performed by a coupled approach which, starting from the results of a global finite element method (FEM) analysis, proceeds through the sub modelling of the cracked volume in a DBEM dual boundary element method (DBEM) environment and subsequent propagation analysis.

**Keywords:** FEM; DBEM; Fracture Mechanics; Turbine rotor blade

## Introduction

Most components in power plant such as turbine rotors have been in service for more than 20 or even 30 years, which is much longer than their design life of 105 h. Now the power steam turbine elements at heat-power engineering enterprises have exhausted their life span or come closer to their limiting values so that a large and growing portion of electricity is produced by ageing thermal power plants.

Turbine disk and blades are subjected to cyclic loading and the structural integrity assessment of these components, with particular reference to remaining life prediction, are increasingly required to guarantee the safe and economic running of power plant engineering components. Extending the life of steam turbines and ensuring high reliability requires life assessment technology, scheduled repairing, modification and upgrading of components in order to provide a stable power supply.

In this paper, we are interested in low-pressure power steam turbine, experiencing in service fatigue failures due to damage accumulation and growth.

Although high quality materials are used for the steam turbines, various forms of metallurgical degradation, like creep and fatigue, affect the parts and components during long-time operation at medium-high temperature.

There are several kinds of examination methods for damage assessment of steam turbines: destructive methods, non-destructive methods and numerical modelling, but they are not always effective and accurate. In order to predict the residual fatigue life of turbine blades, it is necessary to carry out fatigue life and fracture resistance assessment of given material with allowance for the operating time.

This study is concerned with assessment of damage accumulation and growth occurred on the leading edge of a turbine blade, with the crack propagation starting from part-through surface flaws.

A combined FEM-DBEM approach is adopted to calculate the fracture mechanics parameters useful to assess crack growth rates and lifetime of such turbine blades. In particular, the stress analysis on the global model is performed by FEM [1-3] whereas the crack propagation phase is simulated by DBEM [4-7], with the stress intensity factors (SIFs) values along the crack front calculated using the crack opening displacement (COD) method [8-11].

Residual fatigue life of turbine blades could be predicted with reasonable accuracy from knowledge of 3D stress-strain state, SIFs, fracture resistance material properties and in correspondence of different types of operation loadings.

In operation, the analysed blades experiences two main types of damage: the first is the erosive and corrosive pitting, with an initial flaw size approximately equal to 0.5 mm; the second is a welding defect introduced during the protective coating application, on the leading edge of the blade, with an initial flaw size approximately equal to 1.5 mm. The former kind of defect is modelled in this work.

Critical crack lengths discovered on in service blades were varying from 28 to 32 mm.

The analysed blades belongs to the 27$^{th}$ stage of a 200 MW power steam turbine with operation time t=92245 hours. Fatigue failures of blades in rotating turbine disk were detected in service. Their fracture was the result of fatigue crack initiation and propagation up to the formation of a critical crack. In all of these failures, crack propagation started from leading edge as a part-through surface flaw (Figure 1) produced by erosive and corrosive pitting.

## Experimental Tests

Tensile tests were performed for determination of the main mechanical properties of blade materials. Smooth and notched specimens were cut out from critical zones of turbine blade body with given operating time in order to allow for degradation of mechanical properties such as strength and ductility. The material analysed by experimental tests is a steel X20Cr13 bar of circular cross-section with

***Corresponding author:** Citarella R, Department. of Industrial Engineering, University of Salerno, via Giovanni Paolo II, 132, Fisciano (SA), Italy, Tel: +39 089 961111; E-mail: rcitarella@unisa.it

**Received** April 27, 2015; **Accepted** May 26, 2015; **Published** May 28, 2015

**Citation:** Citarella R, Lepore M, Shlyannikov M, Yarullin R (2015) Fatigue Crack Growth by FEM-DBEM Approach in a Steam Turbine Blade. Ind Eng Manage 4: 160. doi:10.4172/2169-0316.1000160

**Citation:** Citarella R, Lepore M, Shlyannikov M, Yarullin R (2015) Fatigue Crack Growth by FEM-DBEM Approach in a Steam Turbine Blade. Ind Eng Manage 4: 160. doi:10.4172/2169-0316.1000160



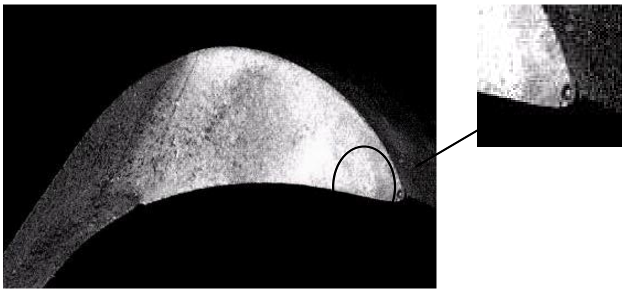

**Figure 1:** Blade post mortem fractographic evidence with highlight of initial defect.

| Turbine Blade (27 stage) | Steel X20Cr13 | Yield stress | Engineering tensile strength | Ultimate tensile strength | Reduction of area | Ultimate strain | Young's modulus |
|---|---|---|---|---|---|---|---|
| | | $\sigma_y$, MPa | $\sigma_t$, MPa | $\sigma_f$, MPa | ψ, % | δ, % | E, GPa |
| Operating time: 0 hours | | 520 | 720 | 1375 | 65 | 21 | 200 |
| Operating time: 92245 hours | | 626 | 760 | 1500 | 69 | 29 | 198 |

**Table 1:** Main mechanical properties of turbine blades material for different operating time.

straight-fronted edge crack.

The optical microscope measurement and the COD (crack opening displacement) method are used to monitor and calculate both crack depth and superficial crack length during the tests. The validity of effective crack length approximation, estimated by continuous measurements of COD data for each fatigue crack path under cyclic loading, is considered.

Growth rate tests were performed with an harmonic test-cycle and as a result, the Paris law calibration was obtained.

In order to determine the influence of operating time on the main mechanical properties of blade material, smooth specimens were cut out from the considered turbine blades.

Experimental study of the material mechanical properties was performed on the uniaxial 25 kN servo-hydraulic tension test machine at room temperature. As a result, the material mechanical property changes were determined as a function of the operating time.

The reference mechanical properties of the blade material with zero operating time and main mechanical properties obtained from tensile tests are listed in Table 1.

Variable amplitude or block tests were realized by repeatedly applying the same loading history on a servo-hydraulic push-pull testing machine with frequency 10 Hz.

## Load sequence

The load sequence used for the fatigue tests on simple specimens has been defined in such a way to be representative of the load history of turbine disk at operation.

It is found that in service, during one year, variable-amplitude fatigue cycles may be approximately clustered in four constant amplitude blocks (Table 2 and Figure 2). The load changes showed in Figure 3 mainly originates from fluid pressure fluctuations but, due to confidential reasons, the real values of stress ratio R in each stage were not disclosed so for experiments and calculation a common (to all stages) value R=0.1 was adopted.

For comparison purposes, fatigue tests were divided into three parts:

- constant amplitude (harmonic) loading;
- variable amplitude loading (block loading when the load history includes four stages on each block);
- spectrum loading with random sequence of the block stages.

The three tests were conducted on a steel bar of circular cross-section with straight-fronted edge notch (Figures 3a and 3b), with load levels such as to cover the crack growth rate range $10^{-8}$-$10^{-6}$ m/cycle.

Table 2 gives the max nominal stress and number of cycles per sequence. Each loading history includes N=198 170 cycles and it is repeated iteratively up to failure.

The random sequence was applied by the testing machine by recalling to a random number generator technique. The algorithm for the generation of the signal is such that the same sequence can be

| Stage | 1 | 2 | 3 | 4 |
|---|---|---|---|---|
| Number of loading cycles | 164434 | 28996 | 4193 | 547 |
| Max nominal stress [MPa] | 251.72 | 253.12 | 254.26 | 255.66 |

**Table 2:** Program loading parameters for simple specimen tests (R=0.1 at each stage).

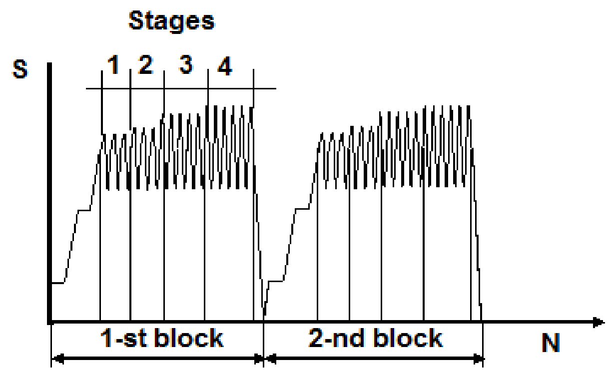


**Figure 2:** Program loading.

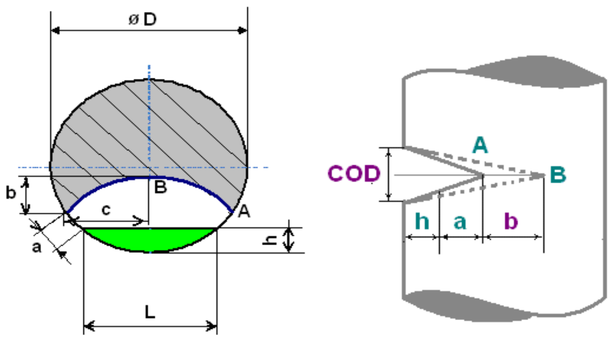


**Figure 3: a-b:** Crack geometric parameters.

**Citation:** Citarella R, Lepore M, Shlyannikov M, Yarullin R (2015) Fatigue Crack Growth by FEM-DBEM Approach in a Steam Turbine Blade. Ind Eng Manage 4: 160. doi:10.4172/2169-0316.1000160



reproduced as many times as desired. Thus the sequence of N=198 170 cycles can be considered as representative of one year operating time for crack growth analysis purpose. Maximum five sequences of about $10^6$ cycles were realized using round bar specimens under pure tension.

## Crack size assessment procedure

Crack growth assessment was performed for the round bar specimens with the straight-fronted edge notch with initial depth $h_0$=0.5 mm [12]. The geometric parameters of specimen test section and growing crack are shown in Figures 3a and 3b. In this Figure 3b is the current crack depth, with the crack front approximated by an elliptical curve with major axis *2c* and minor axis *2b*. The depth of the initial straight edge notch is denoted by *h* and the initial notch length by *L*.

All cylindrical specimens were tested under uniaxial loading with the same stress ratio R=0.1. The tests were carried out under load control and sinusoidal loading form. The crack opening displacements were measured on the free surface of cylindrical specimen by using COD gauge, in the central plane of symmetry as shown in Figure 3b. Thus, the growth rate of the semi-elliptical-fronted edge crack during the fatigue tests was determined using COD measurements and experimental data obtained by using optical microscope. The measured data are reported on a diagram with crack length in the deepest point *b* of the crack front versus accumulated number of cycles *N*. To this end the following approximate equations were used, where *b/D* and *c/D* are the dimensionless crack depth and crack chord respectively:

$$\left(\frac{b}{D}\right)=0.495259\ln\left(\frac{c}{D}\right)+0.861131c \quad \text{- constant amplitude loading}$$

$$\left(\frac{b}{D}\right)=0.512731\ln\left(\frac{c}{D}\right)+0.874907 \quad \text{- variable amplitude loading}$$

$$\left(\frac{b}{D}\right)=0.397675\ln\left(\frac{c}{D}\right)+0.768712 \quad \text{- random loading.}$$

## Results

In Figures 4a and 4b experimental relations between crack opening displacements and crack length on the free surface or cycles are presented; the crack growth curves are obtained under three different test conditions: constant amplitude, variable amplitude and random loading. It is found that the crack growth rates along the external surface direction are similar for different loading conditions.

On the base of this experimental data, polynomial functions were calibrated to express COD as a function of the superficial crack length. Figure 5b shows that variable amplitude cyclic loading leads to an increase of the total fatigue life with respect to constant amplitude cyclic loading.

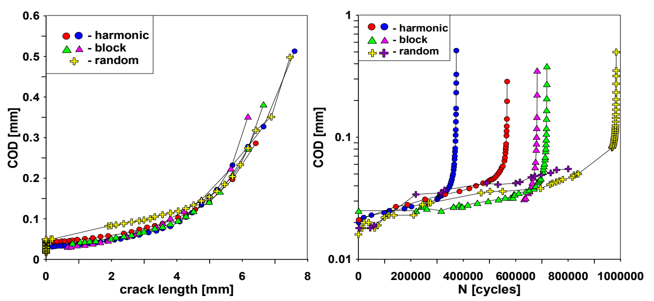


**Figure 4:** COD vs. *a* size (a) and vs. Cycles (b).

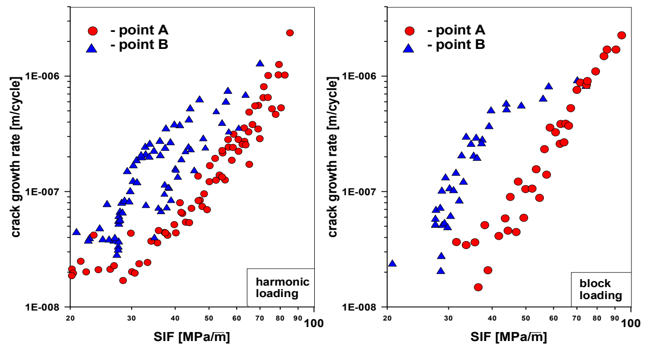


**Figure 5:** Crack growth rate for (a) constant amplitude and (b) variable amplitude loading.

| Material | Crack front position | Constant amplitude loading | | Variable amplitude (block) loading | |
|---|---|---|---|---|---|
| | | C | m | C | m |
| Steel X20Cr13 | Point(·) **A** Free surface | $0.6357\cdot10^{-11}$ | 2.6068 | $0.1987\cdot10^{-11}$ | 2.8765 |
| | Point(·) **B** Mid-section | $0.2207\cdot10^{-10}$ | 2.3722 | $0.7389\cdot10^{-12}$ | 3.4467 |

**Table 3:** Crack growth rate equation (1) parameters (da/dN [m/cycle] and K[MPa × $m^{0.5}$]).

It is well known that total fatigue life can be divided into two stages -crack initiation and growth, therefore, looking at the second stage in Figure 4b and considering the changes in the general durability of the specimens undergoing pure harmonic rather than variable-amplitude loading, significant differences in the crack growth rate in the depth direction *b* under the above types of loading conditions are expected.

Figures 5a and 5b represents the fatigue fracture diagrams with crack growth rate versus SIFs for two main points of the crack front: point A, placed on the free surface of cylindrical specimen, and point B that is the deepest point of the crack front.

The well-known equation of Paris was used for experimental data interpretation in terms of crack growth rates under different loading conditions (but pure mode I crack propagation):

$$\frac{da}{dN}=CK_{I,\max}^{m} \quad (1)$$

where C and m are the experimental parameters of the fatigue fracture diagrams that characterize the material resistance to crack growth under cyclic loading.

The results from block loading are compared with those from constant amplitude cycles in terms of varying Paris law calibration (Table 3): this table shows the experimental values of the constants of Eqn. 1 for the cylindrical specimens with initial crack depth equal to 0.5 mm, tested under different loading history. The results of Table 3 indicate that the constant C and m do not coincide with each other for constant and variable amplitude loading. From this table, it appears that, as expected, loading history affects crack growth rate.

**Citation:** Citarella R, Lepore M, Shlyannikov M, Yarullin R (2015) Fatigue Crack Growth by FEM-DBEM Approach in a Steam Turbine Blade. Ind Eng Manage 4: 160. doi:10.4172/2169-0316.1000160



## FEM-DBEM Approach

### FEM analysis

The crack propagation simulation is performed by using a combined approach that, starting from the results of a global FEM analysis applied to a whole blade sector (ANSYS code is adopted [13]), proceeds through the submodelling of the cracked volume in a DBEM environment (BEASY code is adopted [14]) and subsequent automatic crack propagation.

In this work, a FEM elastic-plastic stress analysis was performed for a turbine disk with blades undergoing operating loading conditions. In Figures 6a and 6b the FE model related to a segment of the turbine rotor, including disk, blades and rivets, is showed. In Figure 6c the contour plot of Von Mises stresses points out the most stressed areas, on the leading edge at the blade root as a consequence of the main centrifugal load; such resultant stress state is related to the 27th stage of turbine rotor undergoing operative regime loading conditions. A picture of a single blade is showed in Figures 6d and 6e.

In operation, turbine disk and blades are subjected to inertia loading caused by rotation of the turbine rotor and stresses due to thermal gradients. Surface-to-surface contact finite elements were used at the contact surfaces between blades, rivets and disk. Bending moment induced by steam pressure was neglected as the value of the bending stresses represent only 0.15% of the stress caused by the inertia loading. The elastic-plastic material behavior was described by a bilinear kinematic hardening model.

### DBEM analyses

From Figure 7 it is possible to see the position and geometry of the initial crack to be introduced in the DBEM submodel (Figure 8a) that is extracted from the global blade FEM model by a *skinning* procedure [15-16]. In Figures 8b-8d the Von Mises stresses on the cracked plate subdomain are showed on the deformed plot: it is clear the blade bending and the typical stress gradients at the crack tips.

Then the Paris law (this time $\Delta K$ rather than $K_{max}$ is adopted with consistent variation of the C value):

$$\frac{da}{dN} = C\Delta K_I^m \qquad (C=1.45e-27 \text{ and } m=2.6068) \qquad (2)$$

with the C and m constants provided by a calibration based on constant amplitude tests on the simple specimens (Table 3) and consistent with crack growth rates expressed by m/cycle and K values by Pa × $m^{0.5}$.

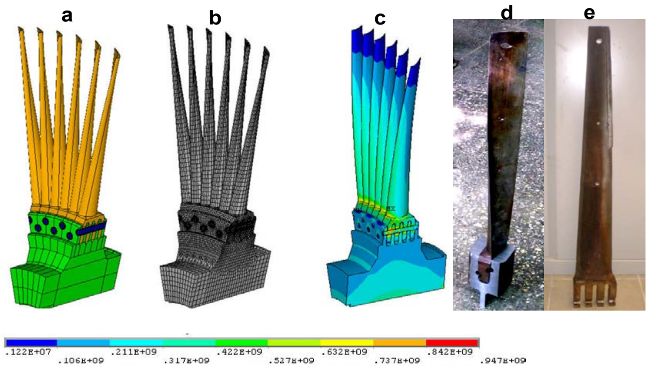


**Figures 6:** Blade sector model: CAD (a), FEM mesh (b), Von Mises equivalent stress (Pa) (c). Single blade picture (d-e).

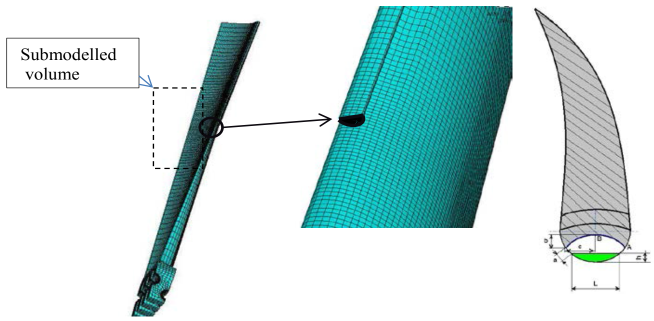


**Figure 7:** Detail of crack initial geometry and position.

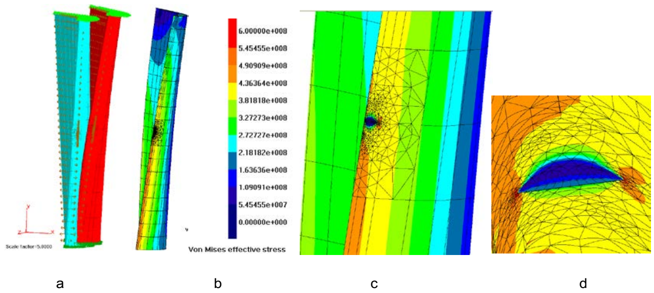


**Figure 8:** DBEM submodel, with highlight of: boundary conditions and deformation (a), Von Mises stresses [Pa] (b), initial crack by external (c) and internal view (d).

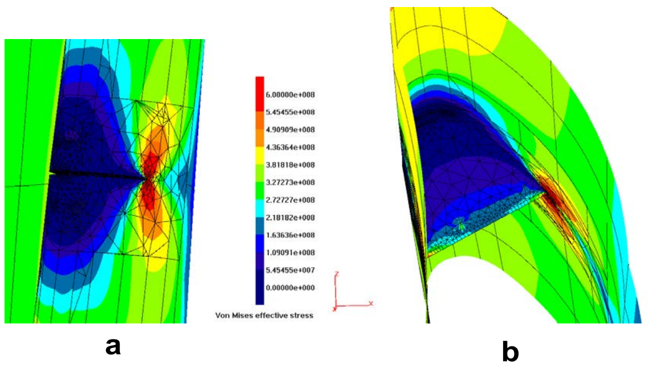


**Figure 9:** DBEM submodel, with highlight Von Mises stresses [Pa] on the finale crack configuration; external (a) and internal (b) view.

The results referred to the surface point A were used because more reliable (the point A advance is directly measured whereas the point B position is reconstructed with a consequent loss of accuracy). SIFs are calculated by the Crack Opening Displacement method because the J-integral approach [17-18] in BEASY code is disabled when centrifugal loads are present.

After 30 steps of crack propagation, using a stress ratio R=0, with a variable average advance in each step (0.2 mm at the beginning and 0.5 mm in the final stage of crack propagation) an unstable condition is reached based on the conservative value of fracture toughness equal to 80 MPa × $m^{0.5}$ (Figures 9a and 9b): the propagation proceeds under pure mode I conditions and that is the reason for only showing the graph with just $K_I$ values (Figure 10). The latter graph shows some irregular fluctuation of $K_I$ values in those parts of crack front close

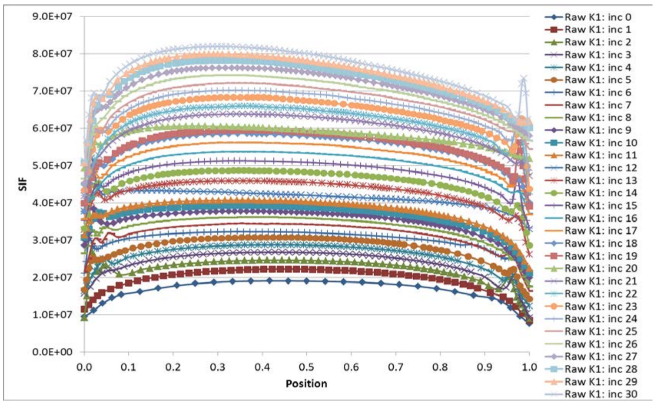


**Figure 10:** $K_I$ values [$Pa*m^{0.5}$] along the crack front at different steps of crack propagation.

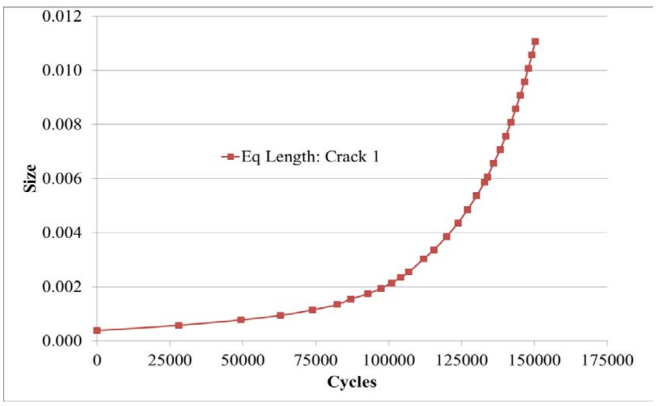


**Figure 11:** Crack depth [m] vs. cycles.

to breakthrough points: this is normal when using COD for SIFs assessment because such technique is highly sensitive to mesh "quality" along the crack front (e.g. quadrilateral elements are better conditioned than triangular…).

In Figure 11 the crack depth vs. Number of cycles is plotted: it clearly shows the sharp acceleration in crack advance in the final stage, when approaching the instability condition.

## Conclusions

In this paper full range of fatigue and fracture resistance characteristics of the turbine blade material was obtained with allowance for the operating time and the accumulated damages. Numerical and experimental results provide the opportunity to predict the residual fatigue life of the power steam turbine blades. The real operational load spectrum acting on the blade was not available so in this work simple switch on/off cycles were considered for the simulation.

It can be emphasized the reduced calculation times of the FEM approach, in comparison with the DBEM approach, the latter providing relevant advantages in the preprocessing phase because the crack insertion and the whole crack propagation is fully automatic, with repeated remeshing realized at each crack step nearly without user intervention.

For the cases analyzed, the functionality of the proposed procedure can be stated.

The adopted procedure can be enriched with the allowance for residual stresses to be directly applied on the crack faces during propagation [19-20].

### References

1. Citarella R, Armentani E, Sepe R, Caputo F (2014) FEM Simulation of a FML Full Scale Aeronautic Panel Undergoing Static Load. Ind Eng Manage 3: 122.
2. Maligno AR, Citarella R, Silberschmidt VV, Soutis C (2015) Assessment of Structural Integrity of Subsea Wellhead System: Analytical and Numerical Study. Frattura ed Integrità Strutturale 31: 97-119.
3. Citarella R, Maligno A, Shlyannikov V (2015) FEM simulation of a crack propagation in a round bar under combined tension and torsion fatigue loading. Frattura ed Integrità Strutturale 31: 138-147.
4. Citarella R and Buchholz FG. Crack growth simulation by BEM for SEN-specimens undergoing torsion or bending loading. Engineering Fracture Mechanics 75: 489-509.
5. Citarella R, Cricrì G (2010) Comparison of DBEM and FEM Crack Path Predictions in a notched Shaft under Torsion. Engineering Fracture Mechanics 77: 1730-1749.
6. Citarella R, Shlyannikov VN, Yarullin R, Lepore MA (2014) Fatigue surface crack growth in cylindrical specimen under combined loading. Engineering Fracture Mechanics 131: 439-453.
7. Citarella R, Perrella M, Lepore M, Cricrì G (2010) DBEM and FEM Analysis of an Extrusion Press Fatigue Failure. Materials with Complex Behaviour-Advanced Structured Materials 3: 181-191.
8. Apicella A, Cariello G, Citarella R, Esposito R (1997) Crack problems by FEM-BEM coupled procedures. The International Journal of BEM Communications 8: 222-229.
9. Calì C, Citarella R, Perrella M (2003) Three-dimensional crack growth: Numerical evaluations and experimental tests. European Structural Integrity Society 31: 341-360.
10. Citarella R, Perrella M (2005) Multiple surface crack propagation: numerical simulations and experimental tests. FFEMS 28: 135-148.
11. Citarella R, Soprano A (2006) Some SIF's evaluations by Dual BEM for 3D cracked plates. Journal of Achievements in Materials and Manufacturing Engineering 19: 64-72.
12. Yang FP, Kuang ZB, Shlyannikov VN (2006)Fatigue crack growth for straight-fronted edge crack in a round bar. International Journal of Fatigue 28: 431-437.
13. Peter Kohenke (1999) ANSYS Theory Reference. 001242 (11thedn.) SAS IP Inc.
14. CM BEASY Ltd. (2011) BEASY V10r14, Documentation.
15. Citarella R, Lepore M, Fellinger J, Bykov V, Schauer F (2013) Coupled FEM-DBEM method to assess crack growth in magnet system of Wendelstein 7-X. Fracture and Structural Integrity 26: 92-103.
16. Citarella R (2014) Thermo-Mechanical Crack Propagation in Aircraft Engine Vane by Coupled FEM-DBEM Approach. Advances in Engineering Software 67: 57-69.
17. Rigby RH, Aliabadi MH (1993) Mixed-mode J-integral method for analysis of 3D fracture problems using BEM. Engng Anal Boundary Elem 11: 239-256
18. Rigby RH, Aliabadi MH (1998) Decomposition of the mixed-mode J-integral-revisited. Int J Solids Struc 35: 2073-2099.
19. Carlone P, Citarella R, Lepore M, Palazzo SG (2014) A FEM-DBEM investigation of the influence of process parameters on crack growth in aluminium friction stir welded butt joints. International Journal of Material Forming.
20. Citarella R, Carlone P, Lepore M, Palazzo SG (2015) In: Carlone, Lepore M, Palazzo GS (eds.) Numerical–experimental crack growth analysis in AA2024-T3 FSWed butt joints. Advances in Engineering Software 80: 47-57.